

Properties of low-lying excited manifolds in the Mn_{12} acetate

Kyungwha Park^{1,2,*} Mark R. Pederson^{1,†} and C. Stephen Hellberg^{1‡}

¹*Center for Computational Materials Science, Code 6390,*

Naval Research Laboratory, Washington DC 20375

²*Department of Electrical Engineering and Materials Science Research Center,*

Howard University, Washington DC 20059

(Dated: May 30, 2018)

Abstract

Most experimental data on the single-molecule magnet Mn_{12} acetate have been successfully explained by the assumption that the Mn_{12} acetate has an effective ground-state spin of $S = 10$. However, the effect of the low-lying excited manifolds caused by interactions between Mn spins has not been well understood. To investigate the features of the low-lying excited manifolds, the intramolecular exchange interactions are calculated using density-functional theory (DFT). With the calculated exchange parameters, the energy gap between the $S = 10$ ground-state and the first excited-state manifold is calculated by diagonalization of the Heisenberg Hamiltonian. The upper limit on the energy gap is about 40.5 K which is likely to be overestimated due to incomplete treatment of the Coulomb potential within DFT. It is found that there are several $S = 9$ low-energy excited-state manifolds above the $S = 10$ ground-state manifold. The magnetic anisotropy barriers for the low-lying spin excitations are calculated using DFT. Based on the calculations, it is found that the anisotropy barriers for the low-lying excited manifolds are approximately the same as that for the ground-state manifold, which is applicable to other single-molecule magnets such as Mn_4 .

PACS numbers: 75.50.Xx, 71.15.Mb, 75.30.Gw, 75.30.Et

I. INTRODUCTION

Single-molecule magnets (SMMs) have been extensively studied for the past decade because of both scientific and practical reasons: macroscopic quantum phenomena¹ and possible utilization as magnetic storage devices.² A prototype of the SMMs is $[\text{Mn}_{12}\text{O}_{12}(\text{CH}_3\text{COO})_{16}(\text{H}_2\text{O})_4] \cdot 2(\text{CH}_3\text{COOH}) \cdot 4(\text{H}_2\text{O})$ (hereafter Mn_{12}),³ which is a three-dimensional array of identical $S = 10$ molecules. Very recently, derivatized Mn_{12} type molecules were successfully deposited on a gold film,⁴ which further enhances the prospects for storing magnetic information in a single molecule. A single molecule of Mn_{12} has four ferromagnetically coupled Mn^{4+} ions ($S = 3/2$) in the cubane and eight ferromagnetically coupled Mn^{3+} ions ($S = 2$) in the crown as schematically shown in Fig. 1. In the ground state, the magnetic moments of the eight Mn^{3+} ions are antiparallel to those of the four Mn^{4+} ions which leads to a total spin of $S = 10$.

So far many interesting features of the SMM Mn_{12} such as magnetization steps in the hysteresis loops,^{5,6} electron paramagnetic resonance (EPR) transitions,^{7,8} and low-energy excitations in inelastic neutron scattering,^{9,10,11} have been well understood by considering each molecule as an object with an effective spin of $S = 10$. However, magnetic susceptibility measurements^{12,13,14} have demonstrated that some experimental data could not be in accord with the $S = 10$ single-spin picture and suggested that the first excited-state manifold may be located at 35 K–40 K above the $S = 10$ ground-state manifold within which the energy barrier to magnetization reversal is 65 K in zero field. Since the first excited-state manifold overlaps with the ground-state manifold above 35 K–40 K, an internal many-spin structure of a single molecule should be included to explain the high-energy experimental data. The dimension of the Hilbert space of this SMM is so large that a simplified eight-spin model with strong Dzyaloshinsky-Morya interaction was first proposed to include many-spin effects by dimerizing two strongly bonded Mn spins.¹⁵ Although this eight-spin model explained some experimental data, it was limited to features below 50 K. At higher temperatures the dimerization scheme breaks down. Later all twelve Mn spins were included in the Heisenberg Hamiltonian and excited-state manifolds were clarified by diagonalization of the Hamiltonian with constraining the fixed energy gap between the first excited-state and the ground-state manifold of 35 K.^{16,17} Nonetheless, there is still a big controversy over the energy gap between the first excited-state and the ground-state manifold, and there has been less exploration

of high-energy features caused by many-spin effects. Here “high-energy” means low-lying excited manifolds above the $S = 10$ ground-state manifold. Recent high-energy inelastic neutron scattering measurements exhibited a broad anomalous peak at 10 K, which may have a magnetic origin (not due to phonons) and could not be rationalized by the $S = 10$ single-spin picture because the first allowed peak by the picture is about 14 K.⁹ More recent high-field EPR measurements revealed that several transitions could not be justified by the $S = 10$ single-spin manifold but that they were well explained if we assumed the $S = 9$ first excited-state manifold to be situated at 10-16 K above the ground-state manifold.¹⁸ Additionally, there have been many attempts to determine the signs and magnitudes of the exchange couplings between Mn ions from different approaches^{16,17,19,20} but no consensus has arisen.

To elucidate the energy gap and examine properties within the low-energy excited manifolds, a single molecule of the Mn_{12} is considered and the exchange interactions between Mn spins are calculated using density-functional theory (DFT), which are presented in Secs. II and III. Our calculated values are compared with those from other groups.^{16,17,19,20} Through diagonalization of the isotropic Heisenberg exchange Hamiltonian with our calculated exchange constants using the Lanczos method,^{21,22} excited-state manifolds are manifested and energy gaps between different manifolds are calculated in Sec. IV. The magnetic anisotropy barriers for low-energy spin excitations are calculated using DFT and the anisotropy barriers for low-lying excited manifolds are discussed in Sec. V. Our conclusions are presented in Sec. VI.

II. DFT CALCULATIONS

Our DFT calculations²³ are performed with spin-polarized all-electron Gaussian-orbital-based Naval Research Laboratory Molecular Orbital Library (NRLMOL)²⁴ which is ideal for studying a single molecule to a small number of unit cells. Here we use the Perdew-Burke-Ernzerhof (PBE) generalized-gradient approximation (GGA) in the exchange-correlation potential.²⁵ Since the SMM Mn_{12} has fourfold symmetry, for fully symmetrized calculations the total number of inequivalent atoms to consider is reduced to $176/4 = 44$. To save geometry-optimization time without losing interesting physical properties, the following simplified form of the SMM Mn_{12} is used: $[\text{Mn}_{12}\text{O}_{12}(\text{HCOO})_{16}(\text{H}_2\text{O})_4]$ (acetic acids and

water molecules of crystallization are not included, and 16 acetates, CH_3COO , are replaced by 16 formates, HCOO). The zero-field total anisotropy barrier for the $S = 10$ ground-state manifold does not change much with this simplification. The total magnetic moment for the ground state was confirmed to be $20\mu_{\text{B}}$, which is in good agreement with experiment and it is stable. Details of the optimization schemes and electronic properties of the optimized geometry for the ground state were discussed elsewhere.²⁶ Hereafter, unless specified, our calculations have been carried out for the above simplified form.

III. INTRAMOLECULAR EXCHANGE INTERACTIONS

The fourfold symmetry and the geometry of a single Mn_{12} molecule indicate that there are three symmetrically inequivalent Mn sites and four different exchange interactions between Mn spins as shown in Fig. 1. To calculate the exchange constants using DFT, it is assumed that the magnetic moments of all Mn ions are aligned along a particular direction (collinear). Then eleven distinctive spin configurations are constructed by reversing magnetic moments of a few Mn ions simultaneously from the $S = 10$ ground-state. (See Table I) For example, a $M_s = 9$ state (M_s is an eigenvalue of the total spin operator S projected along the particular direction) can be built by flipping both one Mn spin in the cubane and another Mn spin in the crown within the $S = 10$ ground state: $M_s = -3/2 \times (3 - 1) + 2 \times (7 - 1) = 9$. There are several ways to construct $M_s = 9$ states with collinear spins that are labeled as 9-b, 9-c, and 9-d in Table I. All of the examined collinear spin configurations are *not* eigenstates of S^2 . Mean-field calculations are not directly applicable to optimizing excited states such as $|S = 9, M_s = 9\rangle$ in Mn_{12} , because those eigenstates are represented by linear combinations of many single Slater determinants. The geometries for the distinctive spin configurations are taken to be the same as that for the ground state except for the proper spin arrangements. It is confirmed that a slightly different initial geometry for the collinear spin configurations does not significantly alter our calculated values of the exchange constants. Since fourfold symmetry is broken for the spin configurations considered, unsymmetrized calculations are required with a total number of 100 atoms. The energies of the spin configurations are self-consistently minimized with a small basis set and fine mesh.²⁷ Our calculations show that the minimized energies range from 0.04 eV to 0.2 eV above the ground-state ferrimagnetic structure. From Ref. 26 it is known that for the $S = 10$ ground state the lowest electronic

excitation is a majority spin excitation between the e_g levels in Mn(3d) states, which is about 0.44 eV (majority LUMO-HOMO gap), and that the energy gap between minority lowest unoccupied molecular orbital (LUMO) and majority highest occupied molecular orbital (HOMO) is ~ 0.89 eV. Comparison of the minimized energies to the LUMO-HOMO gaps indicates that these different spin configurations are lower-energy spin excitations than moving an electron from the majority HOMO to the unoccupied majority (or minority) orbital. Thus they will be called low-energy spin excitations. There are twelve equations to solve for five unknowns (the background energy, E_0 , four exchange constants J_1 , J_2 , J_3 , and J_4) so a least-square-fit (LSF) method²⁸ is used.

Our calculated values of J 's are shown in Table II in comparison with results of other groups. When the minimized energies of the low-energy spin excitations are recalculated using the calculated values of J 's, it is found that they are in good agreement with the DFT-calculated energies as indicated in Table I. Prior to comparison to the results of other groups, let us briefly review the essence of the different approaches from the different groups. In Ref. 19 the value of J_1 was first determined from the experimental data, and then J_2 and J_3 were varied with fixed value of $J_4 = 0$ to reproduce the $S = 10$ ground state. In Ref. 16 the values of J 's were slightly varied from the previously reported values¹⁹ using diagonalization of Heisenberg exchange Hamiltonian to provide the $S = 10$ ground state and the energy gap of 35 K between the ground-state and the $S = 9$ first excited-state manifold. In Ref. 17 the exchange parameters were obtained to reproduce their megagauss experimental data with a constraint of the energy gap of 35 K. In Ref. 20 the LDA+U method was used to include electron correlations between Mn ions, and the values of the intra-atomic Hund's exchange parameter J and the average Coulomb parameter U were determined to obtain the correct magnetic moment for the $S = 10$ ground state. Then the exchange constants were calculated from the values of J and U . Our calculations show that the coupling between one Mn spin in the cubane and another Mn spin in the crown closest to the Mn spin in the cubane, J_1 , is confirmed to be the strongest antiferromagnetic coupling, although its absolute magnitude does not agree among different groups. Our calculated value of J_1 agrees somewhat with those from Refs. 17,20. The coupling between a Mn spin in the cubane and the other type of Mn spin in the crown, J_2 , is confirmed to be weaker antiferromagnetic than J_1 . But the ratio of J_2 to J_1 does not agree among different groups. Our value of J_2 is between the values obtained from Refs. 17,20. The coupling between Mn spins in the cubane, J_3 ,

turns out to be the weakest and is ferromagnetic. The coupling between Mn spins in the crown, J_4 , is weakly antiferromagnetic. Overall, the DFT calculated values are closest to the results obtained from Ref. 17, and they are 20%-40% larger than those from the LDA+U method except for the weakest J_3 . However, they are significantly smaller than the other two reported results from Refs. 16,19. Our calculated values of J' may be overestimated compared to experimental data for the following reasons. It has been found from other SMMs such as Mn_4 [Ref. 29] and V_{15} [Ref. 30] that the DFT-calculated exchange interactions were overestimated by a factor of 2 and 3 compared to the experimental data respectively.^{31,32} This overestimated exchange interactions are due to the fact that the PBE generalized-gradient approximation does not fully treat self-interaction corrections of the localized d states in the Coulomb potential. Proper treatment of the electron correlations in Mn atoms may improve our DFT calculations of the exchange interactions. This is supported by the fact that the LDA+U method produces 20%-40% smaller exchange interactions than our DFT calculations and that the exchange interactions decrease with increasing the value of U in the LDA+U method.²⁰

IV. HEISENBERG EXCHANGE HAMILTONIAN

To calculate the energy gap between the ground-state and the first excited manifold, we use the following isotropic (i.e. no anisotropy) Heisenberg exchange Hamiltonian:

$$\mathcal{H} = \sum_{i < j} J_{ij} \vec{S}_i \cdot \vec{S}_j \quad (1)$$

where the sum runs over all pairs connected by the exchange interactions and the values of the coupling constants J_{ij} labeled in Fig.1 are in Table II. The exchange Hamiltonian is a $10^8 \times 10^8$ matrix, which is too large to diagonalize using currently available computers. Thus, using the fact that M_s is a good quantum number, we classify the total number of the 10^8 states into 45 different constant M_s states such as $M_s = \pm 22, \pm 21, \pm 20, \dots, \pm 10, \pm 9, \dots, \pm 1, 0$. Since we are interested in low-lying excited manifolds, we examine $M_s = -12$, $M_s = -11$, $M_s = -10$, $M_s = -9$, and $M_s = -8$ states only. If the $S = 10$ manifold is the ground state, then the lowest-energy eigenstate of the exchange Hamiltonian with a basis set of all $M_s = -10$ states corresponds to $|S = 10, M_s = -10\rangle$. Additionally the lowest-energy eigenstate of the Hamiltonian with a basis set of all $M_s = -9$ states corresponds to $|S = 10, M_s = -9\rangle$

and it should have the same energy as $|S = 10, M_s = -10\rangle$. The eigenstates with the same S must be degenerate if they belong to the same manifold. The first-excited eigenstate of the Hamiltonian with the basis set of all $M_s = -9$ states corresponds to $|S = 9, M_s = -9\rangle$ if the $S = 9$ manifold is the first-excited manifold above the $S = 10$ ground state. There are a total number of 269148 $M_s = 12$ states, 484144 $M_s = -11$ states, 817176 $M_s = -10$ states, and 1299632 $M_s = -9$ states, 1954108 $M_s = -8$ states.

We diagonalize the full Hamiltonian matrices for the $M_s = -12$, $M_s = -11$, $M_s = -10$, $M_s = -9$, and $M_s = -8$ states using the Lanczos method.^{21,22} A few calculated low-lying energy eigenvalues are shown in Table III. The lowest energy for the $M_s = -10$ states is identical to those for the $M_s = -9$ and $M_s = -8$ states, but it is much lower than the lowest energies for the $M_s = -11$ and $M_s = -12$ states. The lowest energies for the $M_s < -12$ states will increase with increasing $|M_s|$. This indicates that the ground-state has $S = 10$. Next higher energies are from the $M_s = -9$ and $M_s = -8$ states. The three excited energy eigenvalues for the $M_s = -9$ states coincide with those for the $M_s = -8$ states which are much lower than the excited energies for the $M_s = -10$, $M_s = -11$, and $M_s = -12$ states. This suggests that the three excited states for the $M_s = -9$ ($M_s = -8$) states belong to $S = 9$ manifolds. So the first excited-state manifold has $S = 9$ located at 40.5 K above the $S = 10$ ground state, and there are two more $S = 9$ excited manifolds located at 7 K and 40 K above the $S = 9$ first excited manifold (Fig. 2). Our calculated values of the energy gaps are upper limits because DFT calculations may overestimate the exchange interactions due to the reasons discussed in Sec. III. If the exchange constants are reduced by a half, then the energy gaps will be also reduced by a half. Single-ion anisotropy parameters which we did not include in Eq. (1) does not significantly affect the energy gap.

V. MAGNETIC ANISOTROPY BARRIER

The magnetic anisotropy barriers for the eleven low-energy spin excitations as well as the ground state are calculated with the assumption that the barriers are caused by the spin-orbit interaction only. Other effects such as noncollinearity of the magnetic moments of Mn ions and spin-orbit-vibron coupling³³ on the anisotropy barrier will not be included in our study. However correlation effects due to the addition of multideterminantal wavefunctions are addressed in part by the further ongoing discussion. The spin-orbit interaction V_{LS} can

be decomposed into one-electron operators f_i related to the electric fields caused by nuclei and two-electron operators g_{ij} related to the electric fields due to the rest of electrons as follows:

$$V_{LS} = -\frac{1}{2c^2} \sum_i \vec{S}_i \cdot (\vec{p}_i \times \vec{\nabla} \Phi_i) \quad (2)$$

$$= \sum_i f_i + \sum_{i \neq j} g_{ij}, \quad (3)$$

$$\Phi_i = \sum_{\nu} \frac{Z_{\nu}}{|\vec{r}_i - \vec{R}_{\nu}|} + \sum_{j \neq i} \frac{1}{|\vec{r}_i - \vec{r}_j|} \quad (4)$$

$$f_i = \frac{1}{i} \sum_{\nu} \frac{Z_{\nu}}{2c^2} \vec{S}_i \cdot \left(\vec{\nabla}_i \times \frac{(\vec{r}_i - \vec{R}_{\nu})}{|\vec{r}_i - \vec{R}_{\nu}|^3} \right) \quad (5)$$

$$g_{ij} = \frac{1}{i} \frac{1}{2c^2} \vec{S}_i \cdot \left(\vec{\nabla}_i \times \frac{(\vec{r}_i - \vec{r}_j)}{|\vec{r}_i - \vec{r}_j|^3} \right) \quad (6)$$

where the summation for i (ν) runs over all electrons located at \vec{r}_i (all nuclei located at R_{ν} with nuclear number Z_{ν}), c is the speed of light, \vec{S}_i is the spin operator of the i th electron, and \vec{p}_i is the momentum of the i th electron. Within the self-consistent field (SCF) approximation, we have calculated the wave function $\Psi_{i\sigma} = \psi_{i\sigma}(\vec{r})\chi_{\sigma}$ satisfying $\mathcal{H}|\Psi_{i\sigma}\rangle = \epsilon_{i\sigma}|\Psi_{i\sigma}\rangle$, where \mathcal{H} is the many-electron Hamiltonian without spin-orbit coupling, $\psi_{i\sigma}$ is a spatial function and χ_{σ} is a spinor. Therefore, the energy shift, Δ_2 , due to V_{LS} using second-order perturbation theory is written by²⁶

$$\Delta_2 = \sum_{\sigma, \sigma'} \sum_{ij} \frac{\langle \Psi_{i\sigma} | V_{LS} | \Psi_{j\sigma'} \rangle \langle \Psi_{j\sigma'} | V_{LS} | \Psi_{i\sigma} \rangle}{\epsilon_{i\sigma} - \epsilon_{j\sigma'}} \quad (7)$$

where $\epsilon_{i\sigma}$ is the energy of the occupied state with spinor σ , and $\epsilon_{j\sigma'}$ is the energy of the unoccupied state with spinor σ' . The summation runs over all occupied and unoccupied states of all atoms within a certain energy window and over up and down spinor states. The contributions for the cases that both of i and j are occupied (or unoccupied) to the energy shift cancel each other out. For uniaxial systems such as Mn_{12} the second-order energy shift is simplified as follows:

$$\Delta_2 = D \langle S_z \rangle^2 \quad (8)$$

where D is the uniaxial anisotropy parameter which can be calculated from Eq. (7). For the $S = 10$ ground state, as shown in Table I the uniaxial parameter is about 0.54 K, which is in good agreement with experiment.⁷

An eigenstate $|\Phi\rangle$ of the many-electron Hamiltonian that belongs to an excited-state manifold can be written in terms of a linear combination of many Slater determinants: $|\Phi\rangle = \sum_{\mu} C_{\mu} |\Phi_{\mu}\rangle$, where $|\Phi_{\mu}\rangle$ is a single Slater determinant (orthonormal basis function), and some of $|\Phi_{\mu}\rangle$ correspond to our examined low-energy spin excitations. Therefore, the expectation value of the spin-orbit coupling V_{LS} with respect to $|\Phi\rangle$, is decomposed into diagonal and off-diagonal elements such as

$$\langle \Phi | V_{LS} | \Phi \rangle = \sum_{\mu} C_{\mu}^* C_{\mu} \langle \Phi_{\mu} | V_{LS} | \Phi_{\mu} \rangle + \sum_{\mu \neq \nu} C_{\mu}^* C_{\nu} \langle \Phi_{\mu} | V_{LS} | \Phi_{\nu} \rangle, \quad (9)$$

where the summations run over spatial coordinates and spin variables of all electrons in Mn_{12} . V_{LS} is made of one-electron and two-electron operators as shown in Eq. (3). To facilitate calculations of the diagonal and off-diagonal elements, the off-diagonal elements of the one-electron operator, $\sum_i \langle \Phi_{\mu} | f_i | \Phi_{\nu} \rangle$, are explicitly written in terms of single-electron spin-orbitals.³⁴

$$\begin{aligned} \sum_i \langle \Phi_{\mu} | f_i | \Phi_{\nu} \rangle &= \frac{1}{i} \sum_i \int d^3 r_1 \cdots d^3 r_N \sum_{\sigma_1, \dots, \sigma_N} \psi_{1\sigma_1}^*(\vec{r}_1) \chi_{\sigma_1}^* \psi_{2\sigma_2}^*(\vec{r}_2) \chi_{\sigma_2}^* \cdots \psi_{N\sigma_N}^*(\vec{r}_N) \chi_{\sigma_N}^* \\ &\cdot \sum_{\nu} \frac{Z_{\nu}}{2c^2} \vec{S}_i \cdot \left(\vec{\nabla}_i \times \frac{(\vec{r}_i - \vec{R}_{\nu})}{|\vec{r}_i - \vec{R}_{\nu}|^3} \right) \begin{vmatrix} \psi'_{1\sigma_1}(\vec{r}_1) \chi'_{\sigma_1} & \cdots & \psi'_{1\sigma_1}(\vec{r}_N) \chi'_{\sigma_1} \\ \vdots & \ddots & \vdots \\ \psi'_{N\sigma_N}(\vec{r}_1) \chi'_{\sigma_N} & \cdots & \psi'_{N\sigma_N}(\vec{r}_N) \chi'_{\sigma_N} \end{vmatrix} \quad (10) \end{aligned}$$

where $\vec{\nabla}_i$ is also applied to the single-electron spin-orbitals and the normalization factor $1/N!$ cancels out $N!$ permutations of the N single-electron spin-orbitals in $\langle \Phi_{\mu} |$. As can be seen from Eq. (10), because all spin-orbitals $\psi_{1\sigma_1} \chi_{\sigma_1}, \dots, \psi_{N\sigma_N} \chi_{\sigma_N}, \psi'_{1\sigma_1} \chi'_{\sigma_1}, \dots, \psi'_{N\sigma_N} \chi'_{\sigma_N}$, are orthonormal to each other, the off-diagonal elements of the one-electron operator f_i are nonvanishing when only one single-electron spin-orbital is different between $|\Phi_{\mu}\rangle$ and $|\Phi_{\nu}\rangle$. The off-diagonal elements of the two-electron operator g_{ij} are nonvanishing when no more than two single-electron spin-orbitals are different between $|\Phi_{\mu}\rangle$ and $|\Phi_{\nu}\rangle$. Different single Slater determinants (or different low-energy spin excitations) are not connected by the one- or two-electron operators, so $\langle \Phi_{\mu} | V_{LS} | \Phi_{\nu} \rangle = 0$ for $\mu \neq \nu$. Hence, the off-diagonal contributions to the energy shift Δ_2 is zero. As shown in Table I, the calculated magnetic anisotropy barriers for the low-energy spin excitations are almost the same as that for the ground state $S = 10$ manifold. This indicates that the diagonal elements of the spin-orbit interaction [Eq. (9)] do not vary much with different spin excitations: $\langle \Phi_{\mu} | V_{LS} | \Phi_{\mu} \rangle \sim \langle \Phi_{\nu} | V_{LS} | \Phi_{\nu} \rangle$ for $\mu \neq \nu$. Then $\langle \Phi | V_{LS} | \Phi \rangle \sim \langle \Phi_{\mu} | V_{LS} | \Phi_{\mu} \rangle (\sum_{\mu} |C_{\mu}|^2)$ where $\sum_{\mu} |C_{\mu}|^2 = 1$ by

definition. So the magnetic anisotropy barriers for low-lying excited-state manifolds must be approximately the same as that for the ground-state manifold. Note that we have calculated second-order anisotropy barriers only so that the barriers shown in Table I are all between 54 K and 55 K. The results of this discussion suggest that the DFT-based determination of MAE is valid under the following conditions: (i) single-electron and two-electron excitations cost an order of eV, (ii) considered collinear spin excitations cost an order of magnitude less energy than the single-electron and two-electron excitations.

VI. CONCLUSION

We have calculated the intramolecular exchange interactions among Mn spins in the single-molecule magnet Mn_{12} ($[\text{Mn}_{12}\text{O}_{12}(\text{HCOO})_{16}(\text{H}_2\text{O})_4]$) considering localized low-energy spin excitations using density-functional theory. Our calculated values of the exchange constants agree with the results from Refs. 17,20. With our calculated exchange constants, we have diagonalized the isotropic Heisenberg Hamiltonian using the Lanczos method. We have confirmed that the ground state is $S = 10$ and that there is a $S = 9$ first-excited manifold located at 40.5 K above the $S = 10$ ground-state manifold. This energy gap (40.5 K) is an upper limit because it is likely reduced by including more exact treatments of the Coulomb potential or electron correlations. This indicates that the first excited manifold may be situated much lower than the high energy levels within the $S = 10$ ground-state manifold. We have also calculated the magnetic anisotropy barriers for the low-energy spin excitations using DFT and the second-order perturbation theory with the assumption that the spin-orbit coupling is the most important interaction. Our DFT calculations have showed that the anisotropy barriers for the low-energy spin excitations are approximately the same as that for the $S = 10$ ground state. From this result and our understanding of the spin-orbit interaction, we conclude that the anisotropy barriers for the low-lying excited manifolds are approximately same as that for the $S = 10$ ground state.

Acknowledgments

KP was funded by W. M. Keck Foundation, MRP and CSH were supported in part by ONR and the DoD HPC CHSSI program.

- * Electronic address: park@dave.nrl.navy.mil
- † Electronic address: pederson@dave.nrl.navy.mil
- ‡ Electronic address: hellberg@dave.nrl.navy.mil
- ¹ E. M. Chudnovsky and J. Tejada, *Macroscopic Quantum Tunneling of the Magnetic Moment*, Cambridge Studies in Magnetism Vol. 4 (Cambridge University Press, Cambridge, 1998).
- ² C. Joachim, J. K. Gimzewski, and A. Aviram, *Nature (London)* **408**, 541 (2000).
- ³ T. Lis, *Acta Crystallogr., Sect. B: Struct. Sci.* **36**, 2042 (1980).
- ⁴ A. Cornia, A. C. Fabretti, M. Pacchioni, L. Zobbi, D. Bonacchi, A. Caneschi, D. Gatteschi, R. Biagi, U. Del Pennino, V. De Renzi, L. Gurevich, and H. S. J. Van der Zant, *Angew. Chem. Int. Ed.* **42**, 1645 (2003).
- ⁵ R. Sessoli, D. Gatteschi, A. Caneschi, and M.A. Novak, *Nature (London)* **365**, 141 (1993).
- ⁶ J. R. Friedman, M. P. Sarachik, J. Tejada, and R. Ziolo, *Phys. Rev. Lett.* **76**, 3830 (1996).
- ⁷ A. L. Barra, D. Gatteschi, and R. Sessoli, *Phys. Rev. B* **56**, 8192 (1997).
- ⁸ S. Hill, J. A. A. J. Perenboom, N. S. Dalal, T. Hathaway, T. Stalcup, and J. S. Brooks, *Phys. Rev. Lett.* **80**, 2453 (1998); J. A. A. J. Perenboom, J. S. Brooks, S. Hill, T. Hathaway, and N. S. Dalal, *Phys. Rev. B* **58**, 330 (1998)
- ⁹ M. Hennion, L. Pardi, I. Mirebeau, E. Suard, R. Sessoli, and A. Caneschi, *Phys. Rev. B* **56** 8819 (1997).
- ¹⁰ R. Caciuffo, G. Amoretti, A. Murani, R. Sessoli, A. Caneschi, and D. Gatteschi, *Phys. Rev. Lett.* **81**, 4744 (1998).
- ¹¹ I. Mirebeau, M. Hennion, H. Casalta, H. Antres, H. U. Güdel, A. V. Irodova, and A. Caneschi, *Phys. Rev. Lett.* **83**, 628 (1999).
- ¹² A. Caneschi, D. Gatteschi, L. Pardi, and R. Sessoli, in *Perspectives on Coordination Chemistry*, edited by A. F. Williams, C. Florani, and A. E. Merbach (VCH, Basel, 1992).
- ¹³ A. A. Mukhin, V. D. Travkin, A. K. Zvezdin, S. P. Lebedev, A. Caneschi, and D. Gatteschi,

- Europhys. Lett. **44**, 778 (1998).
- ¹⁴ A. M. Gomes, M. A. Novak, R. Sessoli, A. Caneschi, and D. Gatteschi, Phys. Rev. B **57**, 5021 (1998).
- ¹⁵ M. I. Katsnelson, V. V. Dobrovitski, and B. N. Harmon, Phys. Rev. B **59**, 6919 (1999).
- ¹⁶ C. Raghu, I. Rudra, D. Sen, and S. Ramasesha, Phys. Rev. B **64**, 064419 (2001).
- ¹⁷ N. Regnault, Th. Jolicoeur, R. Sessoli, D. Gatteschi, and M. Verdaguer, Phys. Rev. B **66**, 054409 (2002).
- ¹⁸ R. S. Edwards, S. Hill, S. Maccagnano, N. S. Dalal, and J. M. North, cond-mat/0302052 (unpublished).
- ¹⁹ R. Sessoli, H.-L. Tsai, A. R. Schake, S. Wang, J. B. Vincent, K. Folting, D. Gatteschi, G. Christou, and D. N. Hendrickson, J. Am. Chem. Soc. **115**, 1804 (1993).
- ²⁰ D. W. Boukhvalov, A. I. Lichtenstein, V. V. Dobrovitski, M. I. Katsnelson, B. N. Harmon, V. V. Mazurenko, V. I. Anisimov, Phys. Rev. B **65**, 184435 (2002).
- ²¹ J. K. Cullum and R. A. Willoughby, *Lanczos Algorithms for Large Symmetric Eigenvalue Computations* (Birkhauser, Boston, 1985).
- ²² C. S. Hellberg, W. E. Pickett, L. L. Boyer, H. T. Stokes, and M. J. Mehl, J. Phys. Soc. Japan **68**, 3489 (1999).
- ²³ W. Kohn and L. J. Sham, Phys. Rev. **140**, A1133 (1965).
- ²⁴ M. R. Pederson and K. A. Jackson, Phys. Rev. B **41**, 7453 (1990); K. A. Jackson and M. R. Pederson, *ibid.* **42**, 3276 (1990); D. V. Porezag, Ph.D. thesis, Chemnitz Technical Institute, 1997.
- ²⁵ J. P. Perdew, K. Burke, and M. Ernzerhof, Phys. Rev. Lett. **77**, 3865 (1996).
- ²⁶ M. R. Pederson and S. N. Khanna, Phys. Rev. B **60**, 9566 (1999).
- ²⁷ D. Porezag and M. R. Pederson, Phys. Rev. A **60**, 2840 (1999).
- ²⁸ W. H. Press, B. P. Flannery, S. A. Teukolsky, and W. T. Vetterling, *Numerical Recipes*, (Cambridge University Press, Cambridge, 1986).
- ²⁹ D. N. Hendrickson, G. Christou, E. A. Schmitt, E. Libby, J. S. Bashkin, S. Wang, H. -L. Tsai, J. B. Vincent, P. D. W. Boyd, J. C. Huffman, K. Folting, Q. Li, and W. E. Streib, J. Am. Chem. Soc. **114**, 2455 (1992).
- ³⁰ A. Müller and J. Döring, Angew. Chem., Int. Ed. Engl. **27**, 1721 (1988).
- ³¹ K. Park, M. R. Pederson, and N. Bernstein, cond-mat/0307145 (unpublished).

- ³² J. Kortus, C. S. Hellberg, and M. R. Pederson, Phys. Rev. Lett. **86**, 3400 (2001).
- ³³ M. R. Pederson, N. Bernstein, and J. Kortus, Phys. Rev. Lett. **89**, 097202 (2002).
- ³⁴ J. C. Slater, *Quantum Theory of Atomic Structure*, Vol. 1 (McGraw-Hill, New York, 1960), pp. 291-295.

TABLE I: Here $M_s = 6 - c$ denotes $M_s = 6$, where M_s is an eigenvalue of the total spin operator projected along the easy axis and “c” is attached to distinguish between different types of $M_s = 6$ states. From the second column, shown are flipped spins to create low-energy spin excitations relative to the $S = 10$ ground-state labeled in Fig.1, Ising energy expressions, DFT-calculated energies relative to the ground state, ΔE (in units of eV), the energy differences between DFT results and least-square-fit (LSF), $E^{DFT} - E^{LSF}$, and the magnetic anisotropy barriers (MAE) (in units of K).

M_s	flipped spins	Ising Energy	ΔE (eV)	$E^{DFT} - E^{LSF}$ (eV)	MAE (K)
10		$E_0 - 24J_1 - 48J_2 + 27J_3 + 64J_4$	0	-0.0049	54.1
6-c	9	$E_0 - 12J_1 - 48J_2 + 27J_3 + 32J_4$	0.0352	-0.0064	54.8
9-b	1, 9	$E_0 - 24J_1 - 24J_2 + 36J_4$	0.0598	-0.0134	54.5
6-b	5	$E_0 - 24J_1 - 24J_2 + 27J_3 + 32J_4$	0.0780	0.0095	55.2
5-b	1, 5, 9	$E_0 - 24J_1 - 24J_2 + 32J_4$	0.0902	0.0171	54.8
5-a	1, 7, 9	$E_0 - 24J_1$	0.1328	-0.0045	55.4
8-b	1, 4, 5, 9	$E_0 - 12J_1 - 24J_2 - 9J_3 + 36J_4$	0.1361	0.0014	54.1
8	1, 4, 9, 12	$E_0 - 24J_1 - 9J_3$	0.1377	-0.0012	54.9
9-c	4, 5	$E_0 - 12J_1 - 24J_2 + 36J_4$	0.1445	0.0114	54.9
13	1	$E_0 - 12J_1 - 24J_2 + 64J_4$	0.1496	-0.0064	53.6
8-c	1, 8, 9	$E_0 - 12J_1 - 9J_3$	0.1929	-0.0057	54.8
9-d	4, 9	$E_0 - 24J_2 + 32J_4$	0.1955	0.0027	55.0

TABLE II: Comparison of our DFT-calculated intramolecular exchange couplings with those from LDA+U calculations²⁰, diagonalization of the Heisenberg model^{16,17}, and experimental results¹⁹ in units of K. A positive sign denotes an antiferromagnetic coupling.

	DFT	LDA+U[Ref.20]	Ref.17	Ref.16	Exp.[Ref.19]
J_1	115	94	119	430	432
J_2	84	52	118	170	173
J_3	-4	60	-8	170	166
J_4	17	14	23	-129	0

TABLE III: Several lowest-energy eigenvalues of the Hamiltonians for a total number of N $M_s = -12$, $M_s = -11$, $M_s = -10$, $M_s = -9$, and $M_s = -8$ states.

M_s	N	Energy (K)
-12	269148	-2574.2988
-11	484144	-3034.6061
		-2926.5083
-10	817176	-3464.9569
		-3034.6061
-9	1299632	-3464.9569
		-3424.4283
		-3417.4348
		-3384.2171
-8	1954108	-3464.9569
		-3424.4283
		-3417.4348
		-3384.2171

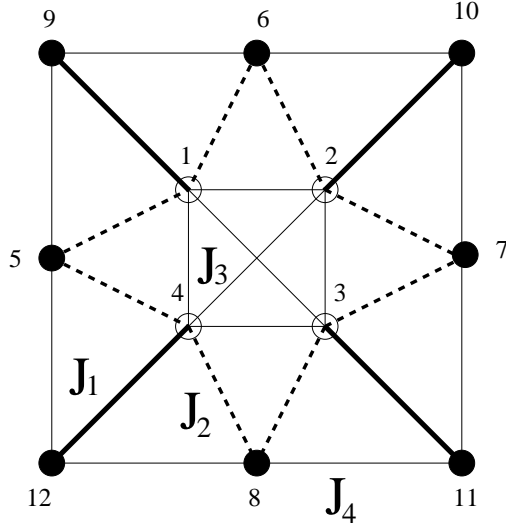


FIG. 1: Schematic diagram of the exchange interactions within a single molecule for the SMM Mn_{12} . The empty circles denote Mn^{4+} ions, the filled circles denote Mn^{3+} ions, and each Mn ion is numerically labeled. The bond length between spin 1 and 9 is shorter than that between spin 1 and 6. The thick solid lines are for J_1 , the thick dashed lines are for J_2 , the thin solid lines in the inner cubane are for J_3 , and the thin solid lines in the outer crown are for J_4 .

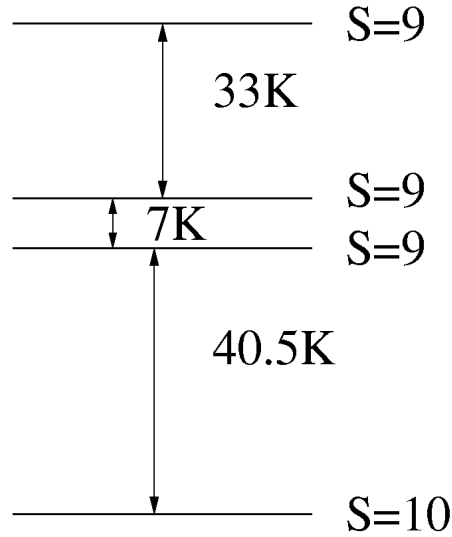


FIG. 2: Calculated low-lying excited manifolds for the SMM Mn_{12} .